sciendo
DOI: 10.2478/rjti-2025-0006
ROMANIAN JOURNAL
OF TRANSPORT INFRASTRUCTURE

COMPARATIVE ASPECTS REGARDING THE BEHAVIOR OF FIBERGLASS AND STEEL REINFORCEMENT IN BRIDGE BEAMS

Amăreanu Marin, Associate Professor, PhD, Technical University of Civil Engineering Bucharest, Faculty of Railways, Roads and Bridges, Department of Roads, Railways and Construction Materials, e-mail: mirel.amareanu@utcb.ro;
Răcănel Ionuț-Radu, Professor, PhD, Technical University of Civil Engineering Bucharest, Faculty of Railways, Roads and Bridges, Department of Strength of Materials, Bridges and Tunnels, e-mail: ionut.racanel@utcb.ro;
Mazilu Claudiu Octavian, Associate Professor, PhD, Technical University of Civil Engineering Bucharest, Faculty of Railways, Roads and Bridges, Department of Roads, Railways and Construction Materials, e-mail: claudiu.mazilu@utcb.ro;
Voinițchi Constantin-Dorinel, Professor, PhD, Technical University of Civil Engineering Bucharest, Faculty of Railways, Roads and Bridges, Department of Roads, Railways and Construction Materials, e-mail: constantin.voinitchi@utcb.ro;
Pirontea George-Mădălin, PhD candidate, Technical University of Civil Engineering Bucharest, Faculty of Railways, Roads and Bridges, Department of Strength of Materials, Bridges and Tunnels, e-mail: george.pirontea@utcb.ro;

Abstract

This study investigates the feasibility of employing fiberglass reinforcement as a substitute for conventional steel reinforcement in concrete bridge beams, with particular attention to mechanical performance and chemical stability within the alkaline environment of concrete.

Keywords: similarity theory; scale model testing; concrete beams; Glass fiber reinforcement polymer (GFRP)

1. INTRODUCTION

The present study aims to highlight the feasibility of using glass fiber reinforcement in bridge beams by estimating the load-bearing capacity of a concrete bridge beam. This research holds significant scientific importance, as it develops a modeling and dimensional analysis framework for scaled-down bridge beams based on similarity theory, comparing beams reinforced with steel and with glass fiber reinforcement. This approach represents a novel contribution to the field of bridge engineering, given that, according to the international literature, experimental testing of scaled bridge beams is rarely addressed [1–5], with most investigations focusing on the derivation of scaling laws using similarity theory for generic beam cases. Moreover, the use of longitudinal glass fiber reinforcement in bridge beams remains limited [6, 7].

By validating this calculation methodology through laboratory testing, the study contributes to technological advancement by simplifying the fabrication, handling, and testing processes of scaled bridge beams, which require relatively small testing forces. Furthermore, it enables a detailed evaluation of the behavior of glass fiber reinforcement bars embedded in bridge beams. Consequently, this approach facilitates the investigation of bridge beam performance under various conditions while reducing the need for costly full-scale physical tests, as scaled models can effectively simulate the structural behavior of real beams.

The experimental approach consists of designing and testing 1:10 scale T-shaped concrete beams, alternately reinforced with steel bars and glass fiber bars, and subsequently evaluated through flexural and shear tests. By applying dimensional analysis based on similarity theory, the findings can be extrapolated to full-scale (1:1) structural behavior.

2. PROTOTYPE BEAM

For the superstructure of a road bridge with a 14.00 m span and a statically determinate simple-beam scheme, a reinforced concrete beam was designed as the prototype.

The prototype was designed as a simple reinforced concrete beam with a T-shaped cross-section, a total length of 15.00 m, and a span of 14.00 m. Concrete class C40/50 was adopted for the calculations.

2.1. Material properties of the prototype beam

The properties of the materials used for the construction of the prototype beam are presented in Table 1 and Table 2.

Table 1. Physical-mechanical characteristics for concrete.

Concrete	
Concrete class	$C40/50$
Characteristic compressive strength of concrete determined on cylinders at 28 days.	$f_{ck} = 40\ MPa$
Partial safety coefficient for concrete, associated with permanent, transient, and seismic loads	$\gamma_c = 1.5$

Design value of concrete compressive strength	$f_{cd} = \frac{f_{ck}}{\gamma_c} = 26.67\ MPa$
Specific weight of reinforced concrete.	$\gamma_{ba} = 25\frac{kN}{m^3}$

Table 2. Physical-mechanical characteristics for reinforcement steel.

Steel in reinforcements	
Steel grade	$S500$
The characteristic flow limit of reinforcements for reinforced concrete	$f_{yk} = 500\ MPa$
Partial coefficient for reinforced concrete or prestressed reinforcement	$\gamma_s = 1.15$
The calculated flow limit of reinforcement for reinforced concrete	$f_{yd} = \frac{f_{yk}}{\gamma_s} =\ 434.783\ MPa$

2.2. Cross-section and geometric characteristics

The cross-section of the beam (Figure 1) was defined in accordance with a standard formwork for prefabricated beams.

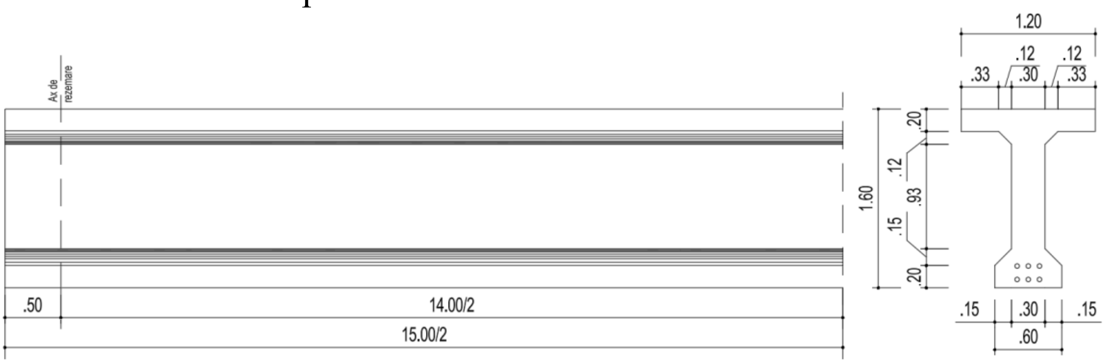

Figure 1. Elevation and cross-section of the prototype beam

Its structural scheme corresponds to that of a simply supported beam (Figure 2).

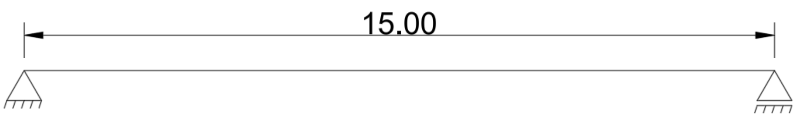

Figure 2. Static scheme

The geometric characteristics of the prototype beam are presented in Table 3.

Table 3. Geometric characteristics of the prototype beam.

Prototype beam area	$A_{gp} = 0.755\ m^2$
Unit weight of reinforced concrete	$\gamma_{ba} = 25\frac{kN}{m^3}$
Prototype beam weight.	$G_{gp} = A_{gp} \cdot \gamma_{ba} \cdot L_{t.gp} = 283.50kN$
Average slab height above beam no. 3	$h_{placa.med} = 0.25m$
Beam height.	$h_{gp} = 1.60m$
Total height of beam and slab	$h_{gp\_placa} = h_{gp} + h_{placa.med} = 1.85m$
Top flange thickness	$h_{tf} = 0.20m$
Top flange width	$b_{tf} = 1.20m$

2.3. Reinforcement design for the prototype beam

The reinforcement design for the prototype beam is presented in Table 4, while the reinforcement layout is shown in Figure 3.

Table 4. Sizing the reinforcement for the prototype beam.

Diameter of longitudinal reinforcement bars	$\Phi_{apr} = 40\ mm$
Area of a single reinforcement bar for flexural moment resistance	$A_{apr} = \pi \frac{\Phi_{apr}^2}{4} = 1256\ mm^2$
Diameter of stirrups	$\Phi_{et} = 10\ mm$
Area of a single reinforcement bar for shear resistance	$A_{et} = \pi \frac{\Phi_{et}^2}{4} = 78.50\ mm^2$
Total reinforcement area for shear resistance	$A_{sw.gp} = 2 \cdot \pi \frac{\Phi_{et}^2}{4} = 157\ mm^2$
Based on crack control requirements, six bars were adopted as the necessary flexural reinforcement., $\Phi_{ar} = 40\ mm$	$A_{apr.total} = 6 \cdot A_{apr} = 7539.822\ mm^2$
Ultimate bending moment capacity of the beam	$M_{Rd} = 4576kN \cdot m$
Ultimate shear capacity of the beam	$V_{Rd} = 1360kN$

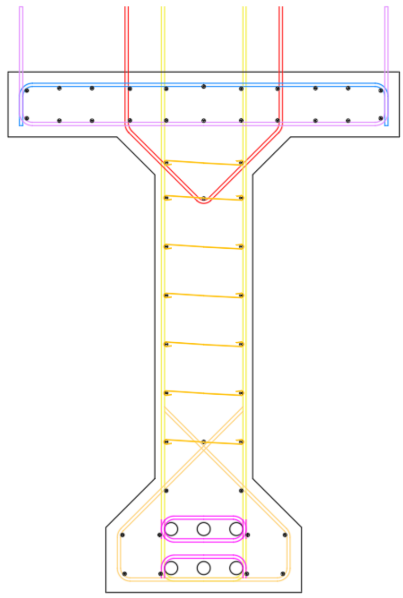

Figure 3. Prototype beam reinforcement plan

3. MATERIALS AND METHODS

3.1. Similarity criteria

The similarity criteria between the prototype beam and the model beam were derived using dimensional analysis based on the Π theorem formulated by E. Buckingham [1,4,5].

According to this theory, any physical process described by n variables can be reduced to a function of the dimensionless criteria Π_1, Π_2, …, Π_{n-r}. The determination of the similarity criteria through dimensional analysis for the selected beam is carried out according to [5], as follows:

- Eight relevant variables are defined (beam weight, force, yield strength, bending moment, reinforcement area, beam height, beam width, and beam span).
- The dimensional matrix is constructed based on the exponents of the fundamental units: mass (kg), length (m), and time (s).
- The rank of the matrix is determined as $r = 3$ ($r \neq 0$), which yields five dimensionless criteria ($n - r = 8 - 3 = 5$).

The expressions of the dimensionless criteria are determined as follows:

- Equations of power products with unknown exponents are formulated.

- A system of equations is obtained to ensure dimensional homogeneity.
- The solution matrix provides the expressions for the five similarity terms Π, as follows:

$$\pi_1 = \frac{M \cdot \sqrt{f_{yk}}}{P \cdot \sqrt{P}}; \quad \pi_2 = \frac{A_s \cdot f_{yk}}{P}; \quad \pi_3 = \frac{h \cdot \sqrt{f_{yk}}}{\sqrt{P}}; \quad \pi_4 = \frac{b \cdot \sqrt{f_{yk}}}{\sqrt{P}}; \quad \pi_5 = \frac{L \cdot \sqrt{f_{yk}}}{\sqrt{P}}$$

The criterial function becomes Ecuation (1):

$$f\left(\frac{M \cdot \sqrt{f_{yk}}}{P \cdot \sqrt{P}}, \frac{A_s \cdot f_{yk}}{P}, \frac{h \cdot \sqrt{f_{yk}}}{\sqrt{P}}, \frac{b \cdot \sqrt{f_{yk}}}{\sqrt{P}}, \frac{L \cdot \sqrt{f_{yk}}}{\sqrt{P}}\right) = 0 \tag{1}$$

The identified criteria allow the determination of the scaling factor as a function of the combination of various parameters involved in this phenomenon. In the present case, the most suitable criterion is the one that expresses the force as a function of the reinforcement area and the ultimate strength (Π_2). Based on the condition that the Π terms are dimensionless, it follows that:

$$\frac{A_s \cdot f_{yk}(u)}{P} = const. \cdots\cdots \Rightarrow \lambda P = \lambda A_s \cdot \lambda f_{yk}(u) \tag{2}$$

The scaling factor λ is obtained as the product of the ratio of reinforcement areas and the ratio of their strengths (prototype versus model).

$$\lambda P = \frac{A_{p,prototip}}{A_{s,\mathrm{mod}\,el}} \cdot \frac{f_{pd,prototip}}{f_{yd,\mathrm{mod}\,el}} \tag{3}$$

The value of the testing force, obtained from the calculation, for the model beam is:

$$P_{\mathrm{mod}\,el} = \frac{P_{prot.}}{\lambda P} \tag{4}$$

3.2. Model beam characteristics

The limitation of the concrete beam cross-section, and consequently of the reinforcement areas Ap (longitudinal reinforcement) and Asw (transverse reinforcement area), restricts the maximum bar diameters used in the experiment to 4 mm. Since ribbed bars with diameters smaller than 6 mm are not available in the construction industry, threaded steel rods and ribbed glass fiber bars (Figure 4.a) were used to simulate the longitudinal reinforcement.

By applying the 1:10 scale reduction parameters, the main characteristics of the model beam are obtained (Table 5).

Table 5. Characteristics of the Model Beam — 1:10 Scale

Concrete class	$C40/50$
Scale reduction coefficient	$\lambda_l = 10$
Total length of the model beam:	$L_{model} = L_{total} / \lambda_l = 1.50\ m$
Diameter of the main longitudinal reinforcement bar for flexural moment resistance – model	$\Phi_{apr.model} = \frac{\Phi_{apr}}{\lambda_l} = 4\ mm$
Area of a single main longitudinal reinforcement bar for flexural moment resistance – model	$A_{apr.model} = \pi \frac{\Phi_{apr.model}^2}{4} = 12.56\ mm^2$
Total area of the main longitudinal reinforcement for the model beam	$A_{apr.total.model} = 6 \cdot A_{apr.model} = 75.36\ mm^2$
Diameter of the transverse reinforcement bar (stirrups) for shear resistance – model	$\Phi_{et.model} = \frac{\Phi_{et}}{\lambda_l} = 1\ mm$
Area of the transverse reinforcement (stirrups) for shear resistance	$A_{sw.model} = 2 \cdot \pi \frac{\Phi_{et.model}^2}{4} = 1.57\ mm^2$
Yield strength of the main longitudinal reinforcement for the model beam	$f_{yk.apr.model} = 330\ MPa$
Design yield strength of the main longitudinal reinforcement for the model beam	$f_{yd.apr.model} = \frac{f_{yk.apr.model}}{\gamma_s} = 287\ MPa$
Yield strength of the transverse reinforcement (stirrups) for the model beam	$f_{yk.etr.model} = 320\ MPa$
Design yield strength of the transverse reinforcement (stirrups) for the model beam	$f_{yd.model.etr} = \frac{f_{yk.etr.model}}{\gamma_s} = 278\ MPa$

a. b.

Figure 4. Reinforcement profile: a. threaded steel rod; b. glass fiber bar

Starting from the prototype beam and applying the scale reduction parameters, the cross-section of the model beam is obtained (Figure 5).

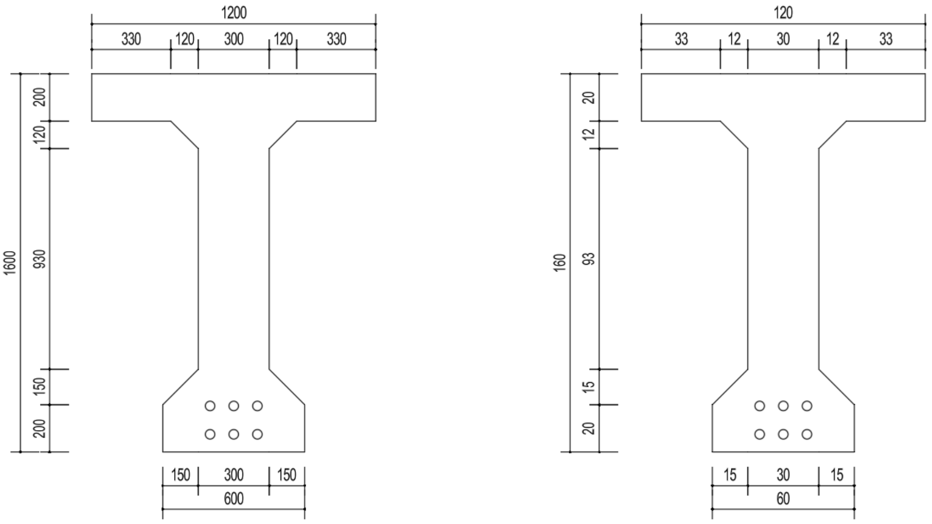

a. b.

Figure 5. Cross-section: a. prototype beam; b. model beam

3.3. Scaling calculations for flexural and shear testing forces

Based on the test configurations illustrated in Figure 6 and Figure 7, together with the maximum bending moment and maximum shear force calculated for the prototype beam, the testing load P required to induce flexural and shear stresses in the model beam is determined as follows:

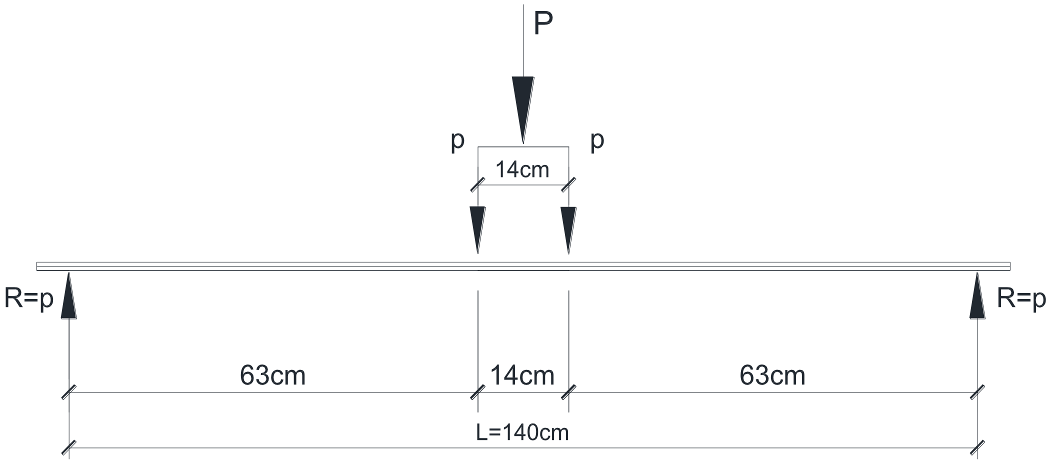

Figure 6. Flexural test setup

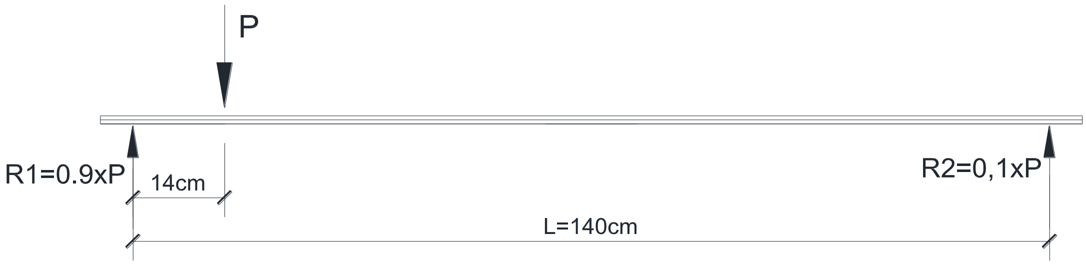

Figure 7. Shear test setup

The load P required for the bending moment test is:

$$P = \frac{M_{Rd}}{a} = \frac{4576kN \cdot m}{6.30m} = 726.35kN \tag{5}$$

$$P_{prototip} = 2P = 1452.7\ kN \tag{6}$$

$$\lambda_p = \frac{A_{apr.total.prototip}}{A_{apr.total.model}} \cdot \frac{f_{yd.prototip}}{f_{yd.model}} = \frac{7539.82}{75.36} \cdot \frac{434.783}{287} = 151.6 \tag{7}$$

$$P_{model} = \frac{P_{prototip}}{\lambda P} = 9.58\ kN \tag{8}$$

The load P required for the shear test is:

$$P_{V.prototip} = \frac{V_{rd}}{0.9} = \frac{1360kN}{0.9} = 1510\ kN \tag{9}$$

$$\lambda P = \lambda A_s \cdot \lambda f_{yk} \tag{10}$$

$$\lambda_p = \frac{A_{sw.gp}}{A_{sw.model}} \cdot \frac{f_{yd}}{f_{yd.model.etr}} = \frac{157}{1.57} \cdot \frac{434.783}{278} = 156.4 \tag{11}$$

$$P_{V.model} = \frac{P_{V.prototip}}{\lambda_P} = \frac{1510}{156.4} = 9.7kN \tag{12}$$

3.4. Concrete mix design

The materials used in the experimental program were selected so that their physical and mechanical properties would closely replicate those of the materials employed in full-scale bridge beam construction. Considering the application of the geometric scaling principle, the cross-sectional dimensions of the beam were significantly reduced, which required the use of a fine aggregate with a maximum particle size of 4 mm for concrete preparation. Regarding the longitudinal reinforcement, small-diameter threaded rods were adopted, chosen in accordance with the criteria of geometric similarity, which involve proportional reduction of both bar diameters and spacing, while ensuring effective composite action with the surrounding concrete.

Starting from the design concrete class used for the prototype beam, a fine-grained concrete was selected as the subject of the research, adapted to the 1:10 scale model. The concrete corresponds to class C40/50 and incorporates continuously graded river aggregate with a particle size range of 0–4 mm.

For the preparation of concrete class C40/50, in accordance with SR EN 206 (Table 6), the following compositional parameters were considered: water/cement ratio = 0.44; water: 242 L (including the admixture); cement content: 550 kg/m^3; river aggregate: 1656 kg; superplasticizer admixture: Sika Plast 302 S, 3% of the cement weight; entrained air: 2%.

Table 6. Materials required for obtaining 1 m³ of concrete.

MATERIAL	PERCENTAGE	QUANTITY (kg)
Cement	550	
Water	242	
AGGREGATE	1656	
Aggregate fraction 2/4	35%	579.6
Aggregate fraction 1/2	20%	331.2
Aggregate fraction 0.5/1	20%	331.2
Aggregate fraction 0.25/0.5	15%	248.4
Aggregate fraction 0/0.25	10%	165.6

Extradur 52 cement was used, which exhibits the following characteristics (Table 7):

Table 7. Characteristics of the cement used.

CEMENT TEST RESULTS (Test method: SR EN 196)			
Cement type		Extradur 52 Cement	
Determination		U.M.	
Standard consistency water		%	30,4
Setting time – beginning		min	200±10
Setting time – end		min	300±14
Soundness		mm	0,0±0.2
Flexural strength	at 2 days	MPa	6,4±0,5
	at 7 days	MPa	8,1±0,5
	at 28 days	MPa	8,6±0,5
Compressive strength	at 2 days	MPa	29,5±1,5
	at 7 days	MPa	47,5±2,3
	at 28 days	MPa	57,8±3,3

The aggregate grading curve was determined by extrapolating the boundary of the granulometric zone corresponding to continuously graded 0/4 mm aggregates, as illustrated in Figure 8. This approach allowed for the selection of an optimal aggregate composition compatible with the requirements imposed by the scaled modeling of bridge beams, while ensuring appropriate physical and mechanical performance within the concrete mixture.

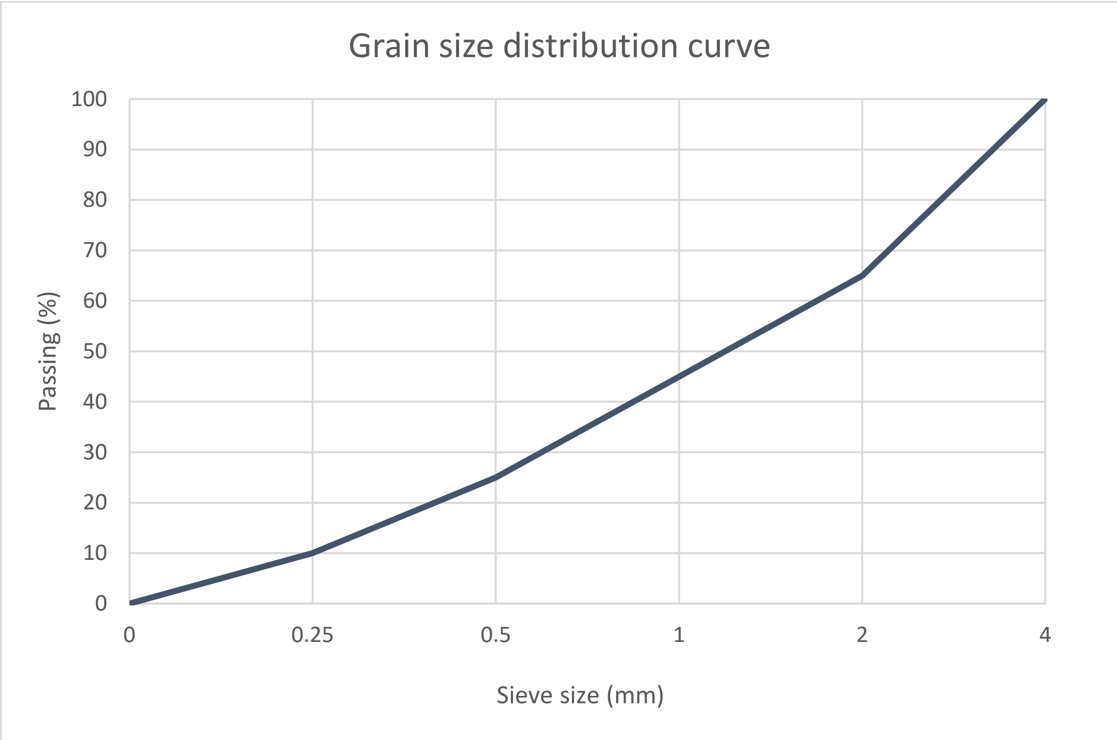

Figure 8. Grain size distribution curve of the aggregate used

The intergranular void volume determined experimentally for the aggregate used was: Vig = 30 %.

To verify the concrete strength class, a batch of 10.125 dm³ of concrete was prepared using the mix proportions presented in Table 6, corresponding to the quantity required for casting three cubes with 15 cm sides. The concrete was placed into the molds with light vibration to prevent segregation.

After 28 days, the cubes were subjected to the compression test, and according to the results presented in Table 8, the target concrete class C40/50 was achieved.

Table 8. Compressive strength of cubes

Test specimens	Cube 1	Cube 2	Cube 3
Compressive strength (fck,cub) N/mm2	50.3	51.4	54.5

3.5. Reinforcement properties (steel and GFRP)

To determine the physical and mechanical properties of the metallic reinforcement bars, tensile tests were carried out (Figure 9) on: two threaded rods, 50 cm in length, with a nominal diameter of 3.80 mm; two smooth wires, 50 cm in length, with a nominal diameter of 1.18 mm.

Figure 9. Tensile testing of reinforcement bars

Figure 10 illustrates the stress–strain diagram corresponding to the two types of reinforcement analyzed, based on which the characteristic strength values specific to each material were determined (Table 9).

Table 9. Tensile strength of steel reinforcement

Test specimens	Threaded rod	Smooth wire (Φ=1.2mm)
Tensile strength ft (N/mm2)	430	375
Yield strength fyk (N/mm2)	330	320

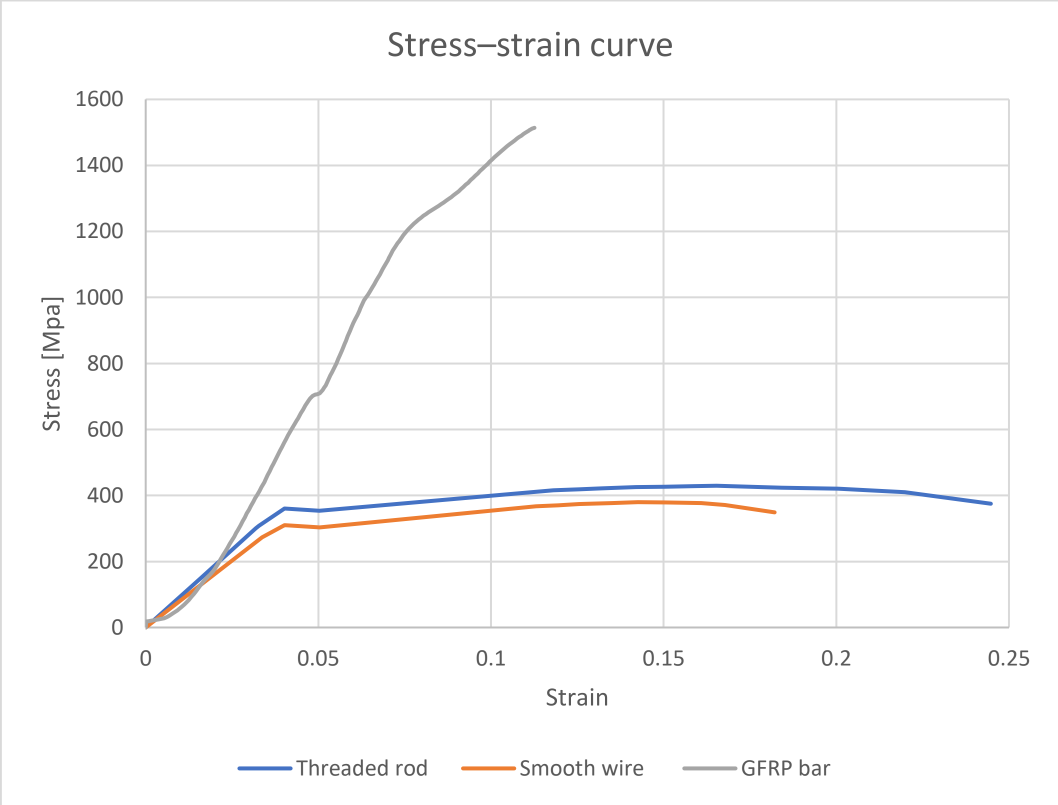

Figure 10. Stress–strain diagram

The loading of the glass fiber reinforcement bars (Φ = 3.8 mm) was carried out according to the setup shown in Figure 9.The experimentally obtained stress–strain diagram, shown in Figure 10, indicates a maximum stress of 1513MPa.

The graphical representations in Figure 10 highlight the distinct mechanical behavior of the reinforcement types, including their failure mode, initial stiffness, and deformation capacity, thereby providing a solid basis for comparing their structural performance in the context of reinforced concrete beam applications. Maximum breaking force for the GFRP stirrup strip: F = 560 N

3.6. Durability testing of GFRP reinforcement in concrete environment

The testing conducted to evaluate the chemical resistance of glass fiber reinforcement in concrete beams aims to validate the chemical behavior of the glass fiber reinforcement in an alkaline environment and to provide a technical basis for the use of glass fiber in the construction of bridge beams.

The testing methodology consisted of the following: Specimens: glass fiber reinforcement bars, Ø4 mm, L = 300 mm; Solution: saturated $Ca(OH)_2$ solution, pH = 13; Immersion temperature: 22 °C; Exposure duration: 90 / 180 / 360 days;

Tensile testing: according to SR EN ISO 15630-1; Visual inspection and mass loss evaluation.

After 180 days of immersion of the glass fiber specimens in a saturated $Ca(OH)_2$ solution with pH = 13, the intermediate microscopic analysis (Figure 11) revealed that the bonding layer remained intact, with no microcracks or visible signs of degradation.

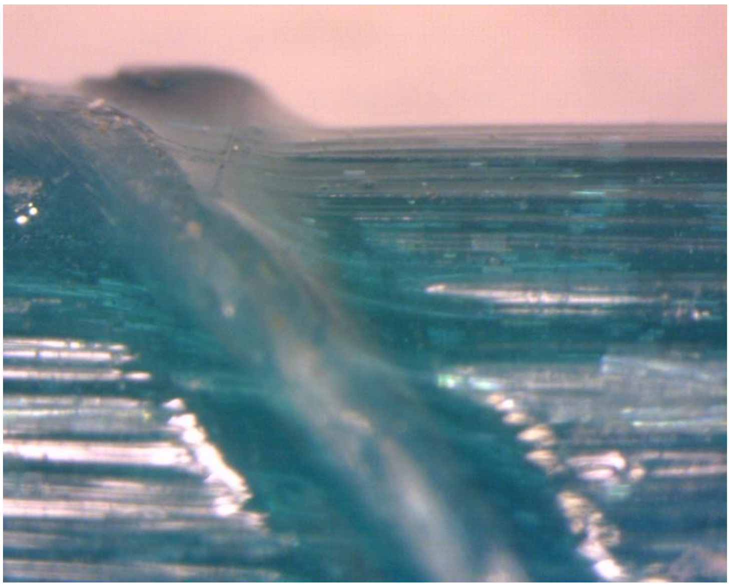

Figure 11. Optical microscopy analysis (200× magnification) of the surface of glass fiber reinforcement bars immersed in $Ca(OH)_2$ solution with pH = 13

Table 10. Intermediate results of the durability test on glass fiber reinforcement bars.

Exposure days	Strength of glass fiber reinforcement bar (%)
0	100
180	100

4. Experimental Program

4.1. Formwork construction

The rigid formworks were made of wooden boards and TEGO panels, accurately reproducing the original geometry of the prototype beam at a 1:10 scale reduction. They were designed to maintain dimensional precision and minimize deformation sensitivity, thereby ensuring the correct positioning of the reinforcement—an essential condition for the validation of the experimental program. Thus, the formwork was designed by adapting the dimensions according to the 1:10 reduction scale, while preserving the geometry of the actual beam (**Figure 12**).

By assembling the components, the formwork shown in **Figure 12**.b was obtained.

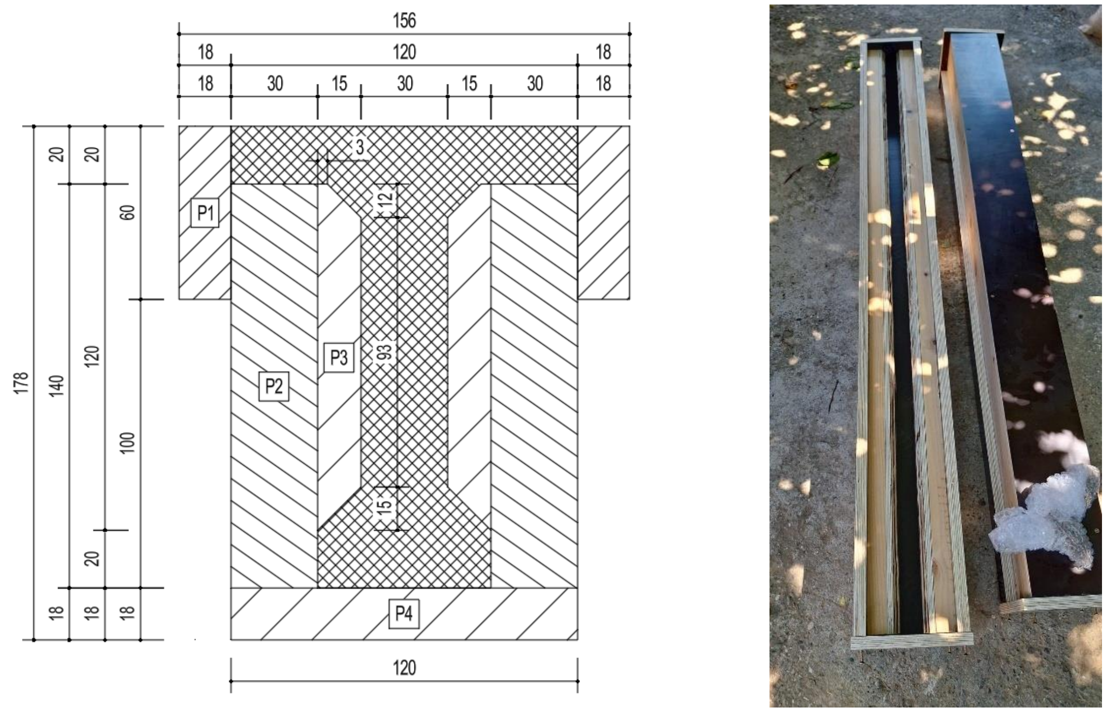

a. b.

Figure 12. Model beam: a. Formwork Layout; b. Formwork Assembly

The accuracy in the formwork execution ensures that the distribution of stresses and internal forces is similar to that of the actual structure.

4.2. Fabrication of reinforcement cages (steel and GFRP) and their placement in the formwork

The reinforcement cages were fabricated according to the reinforcement layout of the prototype beam. The stirrups were produced at a 1:10 scale (Figure 13).

Figure 13. Stirrups

The stirrups were mounted onto the longitudinal bars while maintaining the specified spacing between them. The stirrup spacing, s, Equation (13), was determined based on the reinforcement plan of the prototype beam.

$$s_{gr,\mathrm{model}} = \frac{s_{gr,prototip}}{\lambda_L} = \frac{s(mm)}{10} \tag{13}$$

The fabrication and positioning of the reinforcement cages within the formwork are illustrated in Figure 14.

Figure 14. Details of reinforcement cage fabrication and placement in the formwork

To ensure safe demolding without the risk of surface spalling or other damage, and to prevent water absorption from the concrete, a layer of oil was applied to the formwork surfaces in contact with the concrete.

4.3. Realizarea grinzilor model:

A total of 30 dm³ of fine-grained concrete, with the composition described in Section 3.4, was prepared for casting two beams—one reinforced with conventional steel and the other with glass fiber reinforcement (Figure 15)—as well as two reference cubes.

After three days, the beams were demolded, the formworks were cleaned, and the procedure was repeated for casting additional sets of beams.

Figure 15. Fabrication of model beams

4.4. Testing of Model Beams

The testing of the model beams aims to evaluate their structural behavior under applied loading, focusing on bending moment and shear force response, through static loading under controlled conditions (Figure 16 and Figure 17). The objective is to identify the deformation zones, the formation of cracks, the load-bearing capacity, and the failure mode.

Figure 16. Flexural load test

Figure 17. Shear load test

5. RESULTS

The failure load values of the scaled beams, reinforced with conventional steel and with glass fiber, tested under bending moment and shear force, are presented in Table 11.

Table 11. Failure load values of the scaled beams

Type of test:	Calculated force value (kN)	Failure load value for the model beam (kN):	
		Conventional reinforcement	Glass fiber reinforcement
Flexural load test	9.50	12.20 / 14.30	19.40 / 22.30
Shear load test	9.70	13.80 / 15.40	21.20 / 23.30

The structural behavior of the scaled beams subjected to progressive vertical loading, illustrated through the load–deflection curve, is presented in Figure 18 and Figure 19. The load–deflection relationship highlights the key behavioral stages—from initial stiffness to failure—allowing the identification of critical phases of the structural response, with direct implications for the design and assessment of load-bearing capacity.

Figure 18. Load–deflection curve for the conventionally reinforced steel beam

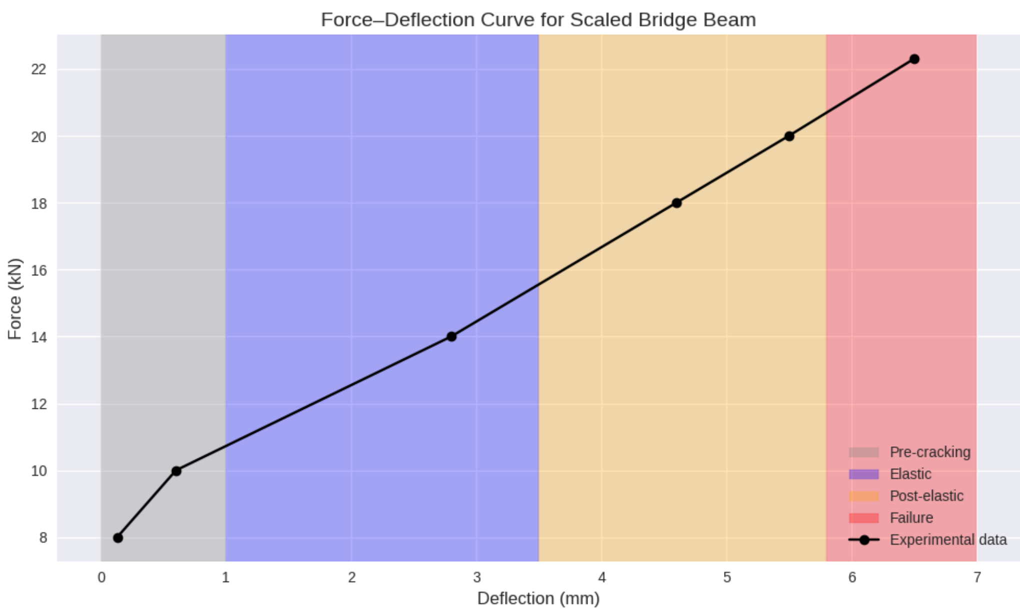

Figure 19. Load–deflection curve for the GFRP reinforced beam

A ductile behavior is observed for both the beams reinforced with conventional steel and those reinforced with GFRP (Figure 18 and Figure 19), showing a gradual progression toward failure, which is favorable from the perspective of structural safety.

The failure modes of the beams subjected to shear force and bending moment are illustrated in Figure 20 and Figure 21.

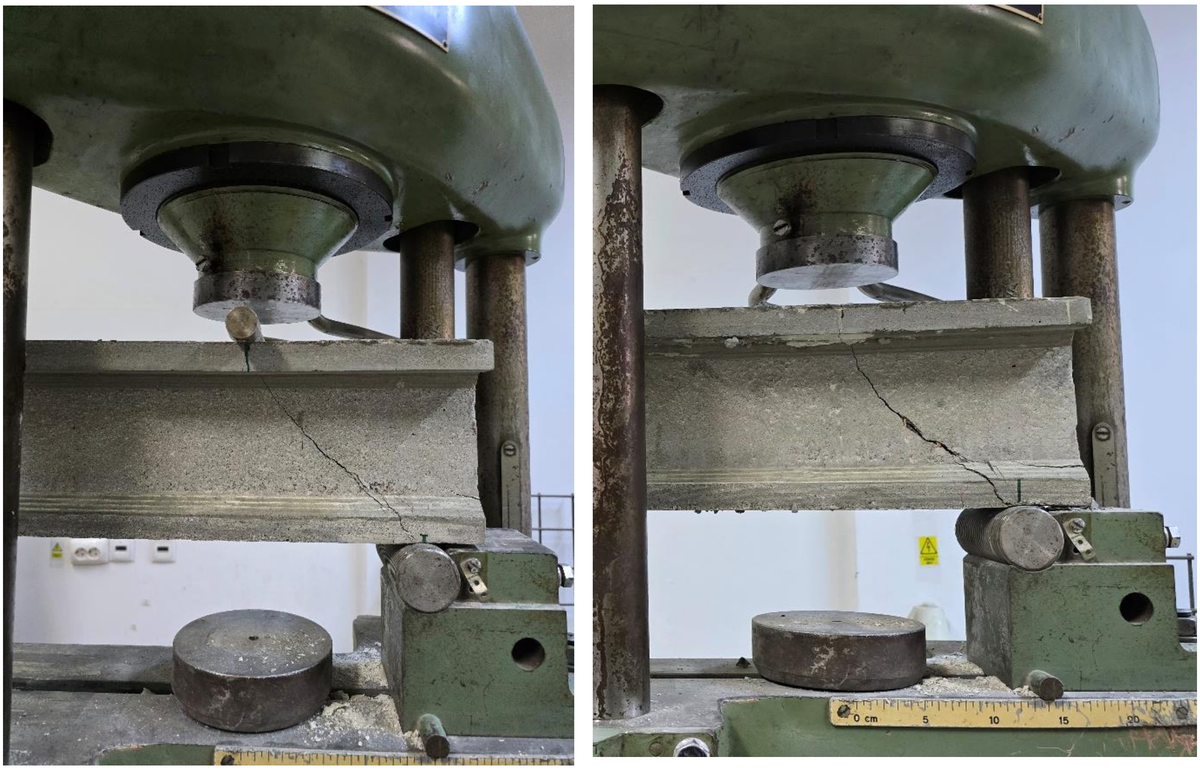

a. b.

Figure 20. Comparison of shear failure mode: a. steel reinforcement; b. GFRP reinforcement

a.

b.

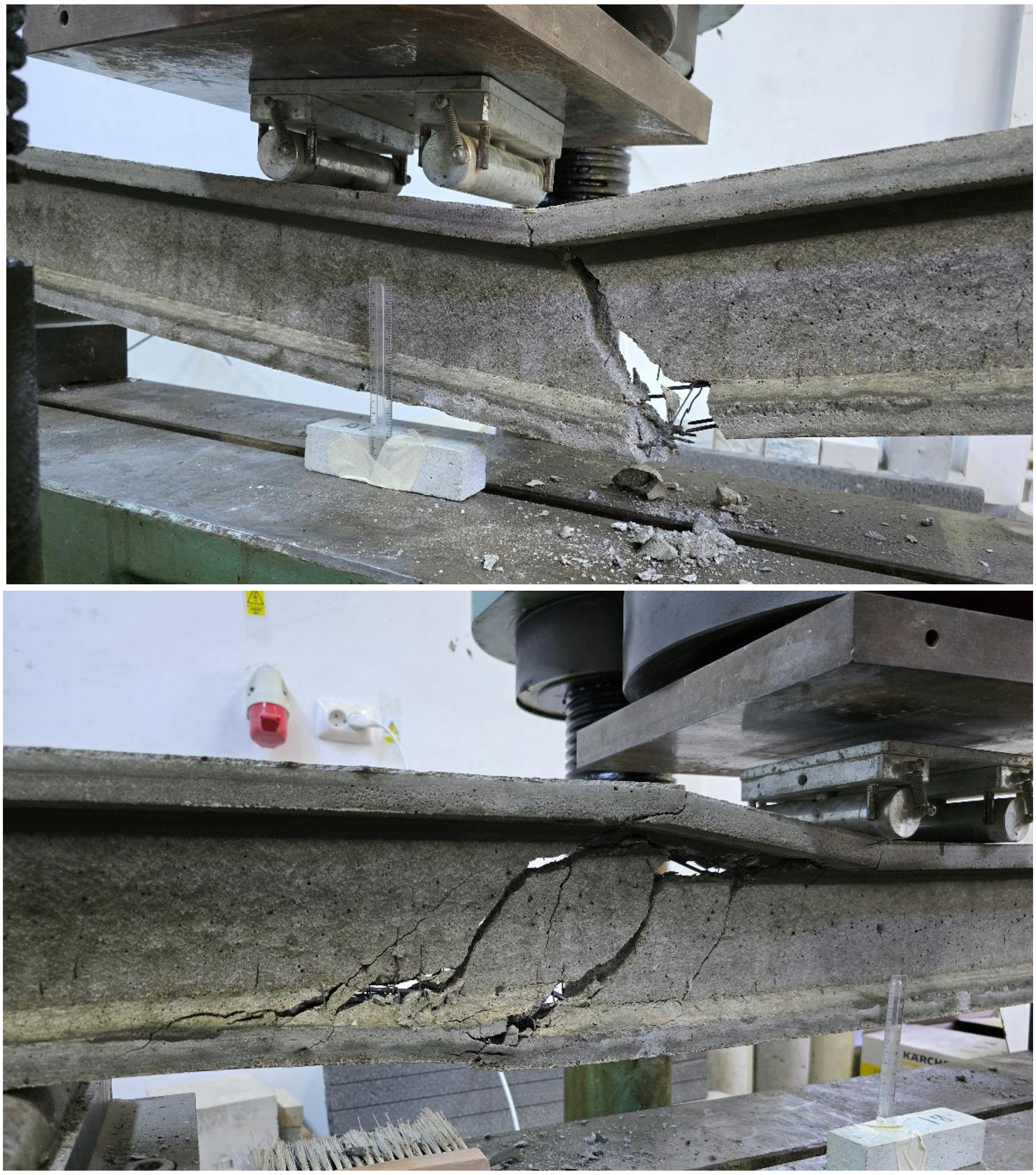

Figure 21. Comparison of flexural failure mode: a. steel reinforcement; b. GFRP reinforcement

The particular features of the cracking mechanism and the evolution of the structural degradation process can be observed depending on the type of loading.

6. DISCUSSION

The shear failure mechanism was similar for both types of reinforcement, as shown in Figure 21. However, in the case of the beams reinforced with GFRP bars, a more dominant and wider crack was observed, which can be attributed to the lower bond strength between the GFRP reinforcement and the concrete.

Flexural loading revealed different failure behaviors between the beams reinforced with conventional steel and those reinforced with GFRP.

Due to the ductile behavior of the steel reinforcement, the conventionally reinforced beams exhibited significant deformations prior to reaching the failure state (Figure 19). The steel reinforcement provides an efficient transfer of tensile stresses, contributing to the control of the cracking process and the limitation of its propagation, as also reported in [8–11].

The failure process initiated with the formation of an initial small, diagonally oriented crack located in the tensile zone of the beam. As the load progressively increased, the crack extended and deepened within this region, ultimately leading to the failure of the element. After failure, no signs of concrete crushing were observed in the compression zone (the upper flange of the beam), indicating good structural performance in this area (Figure 21.a).

As a result of the high ductility of the steel reinforcement, the beam retained its load-bearing capacity even after the initiation of cracks in the concrete, allowing it to sustain considerable loads until the ultimate strength of the reinforcement was reached.

In Figure 21.a, when the loading continues beyond the value corresponding to the onset of concrete cracking, the failure of the steel reinforcement can be observed, following its plastic (ductile) deformation in the tensile zone. In this case, the two parts of the beam resulting after failure remain relatively unaffected.

In the case of GFRP reinforcement, the failure process begins with the formation of a network of microcracks in the tensile zone, which progressively develops as the applied load increases. In Figure 21.b, dominant and deep diagonal cracks can be observed, along with signs of concrete surface spalling in the compression zone. These phenomena are attributed to the reduced bond strength between the GFRP bars and the concrete, as well as to the limited deformation capacity of this type of reinforcement. The failure mechanism of the beams reinforced with GFRP bars, illustrated in Figure 21.b, is characterized by a brittle behavior, without any preceding plastic deformation phase. A significantly more pronounced degradation of the beam can be observed, primarily due to the lack of ductility of the GFRP reinforcement (resulting from the brittle behavior of glass), correlated with the good anchorage within the concrete matrix and the higher individual tensile strength compared to the beams reinforced with steel bars.

The use of glass fiber–reinforced polymer (GFRP) bars in the reinforcement of concrete beams resulted in a significant improvement in the mechanical performance of the tested elements. According to the results presented in Table 11, the ultimate load value increased by approximately 33% to 37% in the beams reinforced with GFRP compared to those conventionally reinforced with steel, both in the flexural and shear tests.

The beams reinforced with conventional steel, as well as those reinforced with glass fiber–reinforced polymer (GFRP) bars, exhibited a gradual and controlled failure behavior, characterized by the appearance of fine, small cracks distributed over the surface of the structural element.

As in the study [5], the experimental results obtained from the flexural and shear tests performed on the scaled models confirmed the relevance of applying the Similarity Theory as an effective method for estimating the structural behavior of real-scale elements.

The application of the scaling factor corresponding to the flexural failure load led to an estimated value of $P_{\text{model},M} = 9.5$ kN. Experimental observations confirmed this prediction, with the actual failure of the conventionally reinforced model occurring at load values ranging between 12.3 and 14.3 kN.

In the shear tests, the failure of the scaled, conventionally reinforced models occurred at load values ranging between $P_{\text{model,cracks}} = 13.8$ kN **și** $P_{\text{model,cracks}} = 15.4$ kN. In comparison, the theoretically estimated value, obtained by applying the scaling factor to the prototype beam's failure load, was $P_{\text{model},V} = 9.7$ kN**.**

The results indicate a satisfactory agreement between the analytical prediction and the structural behavior observed in the laboratory.

7. CONCLUSIONS

Considering the small deviation between the experimental values and those estimated through the application of similarity criteria, it can be concluded that the selected scaling parameters were appropriate for estimating the structural behavior of the prototype element.

The experimental data were analyzed to characterize the structural behavior of concrete beams reinforced with both conventional steel and glass fiber–reinforced polymer (GFRP) bars. The analysis focused on the relationship between the applied load and vertical deformation, the cracking process, and the identification of failure mechanisms associated with each type of reinforcement.

In addition, the post-peak behavior—specific to the loading stage following the attainment of the ultimate load-bearing capacity—was evaluated to highlight the differences in ductility and structural resilience between the two reinforcement systems.

All the analyzed beams exhibited pronounced initial stiffness, indicating an elastic behavior in the early loading phase, characterized by increasing load accompanied by small deflections, consistent with the longitudinal reinforcement configuration shown in Figure 10.

The subsequent structural behavior differs significantly depending on the type of reinforcement used. In the case of beams reinforced with glass fiber–reinforced polymer (GFRP) bars, the attainment of the maximum load (33–37% higher than that of conventionally reinforced beams) was followed by a sudden failure marked by the detachment of the concrete from the reinforcement—a typical brittle behavior associated with reduced ductility. This characteristic limits the ability to redistribute internal stresses and prevents the beam from sustaining additional loads after reaching the ultimate strength.

In contrast, the steel-reinforced beams exhibited superior ductility, allowing the development of significant plastic deformations and ensuring a more favorable post-peak structural response.

The durability of reinforced concrete structures is significantly affected by the corrosion of steel reinforcement, particularly in aggressive environments such as marine or industrial settings. In this context, glass fiber–reinforced polymer (GFRP) reinforcement represents a promising alternative, offering both high tensile strength and corrosion resistance.

This study confirms the potential of glass fiber–reinforced reinforcement for application in road infrastructure.

However, since GFRP exhibits certain limitations related to its brittle behavior and lower elastic modulus, further research is proposed on the combined use of steel and glass fiber reinforcement. Such a hybrid approach could optimize structural performance, ductility, load-bearing capacity, and overall durability.

REFERENCES

[1]. E. BUCKINGHAM, "*On Physically Similar Systems; Illustrations of the Use of Dimensional Equations*" Physical Review, Vol. 4, No. 4, **1914**, pp. 345-376.

[2]. B. R. SEETHALAKSHMI, SRINIVAS VOGGU, "*Dynamic Similitude Analysis for Establishing Scaled-Down Model to Predict Vibration Behavior of Precompressed Concrete Bridge Girder*", Iranian Journal of Science and Technology, Transactions of Civil Engineering volume 47, pages 1629–1641.

[3]. XIAOYAN LEI , ZHENGUO WANG, KUN LUO, "*Design, Verification, and Test of the Bridge Structure Vibration Similarity Model*", Journal of Aerospace Engineering, **Volume 34, Issue 1**

[4]. ALI M. SYED, MOHAMMAD JAVED, BASHIR ALAM, "*Similitude Analysis of Concrete Scaled Bridge Columns for Quasi-Static and Free Vibration Testing*", Journal of Mechanical and Civil Engineering (IOSR-JMCE) Volume 3, Issue 6 (Nov-Dec. **2012**), PP 42-48.

[5]. M. AMAREANU, I.R. RACANEL, C.N. NEACSU, D.D. MORLOVA, "*Laboratory Scaled-Down Cementitious Concrete Model Used for Estimating the Bearing Capacity of a Bridge Girder Based on the Similitude Theory* "– Materials **2023**,16(24), 7559;

[6]. MUHAMMAD HAMMAD, ALIREZA BAHRAMI, SIKANDAR ALI KHOKHAR,RAO ARSALAN KHUSHNOOD, "*A State-of-the-Art Review on Structural Strengthening Techniques with FRPs*" – Materials (Basel), **2024**,17(6):1408. doi: 10.3390/ma17061408

[7]. EHAB A. AHMED, M.ASCE ; BRAHIM BENMOKRANE ; MAXIME SANSFAÇON, "*Case Study: Design, Construction, and Performance of the La Chancelière Parking Garage's Concrete Flat Slabs Reinforced with GFRP Bars*", **2017**, Journal of Composites for Construction, https://doi.org/10.1061/(ASCE)CC.1943-5614.0000656

[8]. .LU, C.; CAI, Q.; XU, K.; SHA, X.; YAN, Y. "*Comparison of Flexural Behaviors between Plain and Steel-Fiber-Reinforced Concrete Beams with Hybrid GFRP and Steel Bars"* Structures **2022**, 43, 1–11.

[9]. ABADEL, A.A. "*Flexural Behaviour of RC Beams with a UHPFRC Top Layer and Hybrid Reinforcement of Steel and Glass Fiber Reinforced Polymer Bars. Case Stud.*" Constr. Mater. **2024**, 21, e04017.

[10]. FENG, C.; LU, C.; WANG, J.; QIAN, H.; YAN, Y. "*Shear Resistance and Calculation Method of GFRP-Reinforced Concrete Beams with CFRPMeshFabric as Shear Reinforcement. Case Stud.*" Constr. Mater. **2024**, 21, e03904.

[11]. P. DZIOMDZIORA , P. SMARZEWSKI, "*Reinforced Concrete Beams with FRP and Hybrid Steel–FRP Composite Bars: Load–Deflection Response, Failure Mechanisms, and Design Implications"*, Materials **2025**, 18, 4381 https://doi.org/10.3390/ma18184381

Acknowledgement
This work was supported by a National Research Grants of the UTCB, ARUST, project number 1393 / 07. 02. 2025